

1 Article

2 **Impact of AVHRR channel 3b noise on climate data**  
3 **records: Filtering method applied to the CM SAF**  
4 **CLARA-A2 data record**

5 **Karl-Göran Karlsson<sup>1,\*</sup>, Nina Håkansson<sup>1</sup>, Jonathan P. D. Mittaz<sup>2</sup>, Timo Hanschmann<sup>3</sup> and Abhay**  
6 **Devasthale<sup>1</sup>**

7 <sup>1</sup> Swedish Meteorological and Hydrological Institute, Folkborgsvägen 17, SE-601 76 Norrköping, Sweden

8 <sup>2</sup> University of Reading, United Kingdom

9 <sup>3</sup> Deutscher Wetterdienst, Offenbach, Germany

10 \* Correspondence: Karl-Goran.Karlsson@smhi.se;  
11 Tel.: +46 11 4958407; Fax: +46 11 495 8001

12 Academic Editor: name

13 Received: date; Accepted: date; Published: date

14 **Abstract:**

15 A method for reducing the impact of noise in the 3.7 micron spectral channel in climate data  
16 records derived from coarse resolution (4 km) global measurements from the Advanced Very High  
17 Resolution Radiometer (AVHRR) data is presented. A dynamic size-varying median filter is  
18 applied to measurements guided by measured noise levels and scene temperatures for individual  
19 AVHRR sensors on historic NOAA polar orbiting satellites in the period 1982-2001. The method  
20 was used in the preparation of the CLARA-A2 data record, a cloud climate data record produced  
21 by the EUMETSAT Satellite Application Facility for Climate Monitoring (CM SAF), as well as in the  
22 preparation of the corresponding AVHRR-based datasets produced by the ESA project  
23 ESA-CLOUD-CCI. The impact of the noise filter was equivalent to removing an artificial  
24 decreasing trend in global cloud cover of 1-2 % per decade in the studied period, mainly explained  
25 by the very high noise levels experienced in data from the first satellites in the series (NOAA-7 and  
26 NOAA-9).

27

28 **Keywords:** AVHRR; climate data record, 3.7 micron channel; noise filtering, CM SAF,  
29 ESA-CLOUD-CCI.

30

31 **1. Introduction**

32 Satellite-based climate data records **have** become increasingly important for climate monitoring  
33 and climate change studies because of their **increasing** maturity and their gradually increasing  
34 length of their **ir** covered observation period. **Especially** ~~the~~ the latter circumstance leads **especially** to  
35 better confidence in the determination of climate trends as well **and also as to a strengthening for**  
36 **increasing of** the overall statistical significance as a climate data record. But the increasing length of  
37 data records inevitably leads to variations in the quality of data due to factors such as changes in the  
38 behaviour of individual sensors and/or changes in sensor design where original spectral channels  
39 (often called “heritage channels”) only exist as a sub-set of all channels. This could then lead to new  
40 problems since the revised sensor performance (often clearly improved compared to predecessors in  
41 terms of stability and signal to noise ratio) can be misinterpreted as an artificial trend or  
42 discontinuity in the long-term measurement series. In conclusion; the longer measurement series we

43 have for one sensor or sensor family, the more we have to work with mitigation methods to avoid  
44 introducing artificial trends in climate data records.

45  
46 The work with homogenization of climate data records is an immense task and it has many  
47 aspects which need consideration depending on the sensor or sensor family. In this paper we want  
48 to highlight one particular feature which is specific to climate data records based on the Advanced  
49 Very High Resolution Radiometer (AVHRR, [1]). The feature to be discussed is the impact of  
50 radiometric noise in AVHRR channel 3b at 3.7 micron on AVHRR-derived climate data records. The  
51 noise problem, producing herring-bone patterns of quite varying intensity in images, was ~~early~~  
52 identified early as a potential problem for climate monitoring applications (e.g., [1], page 101: “The  
53 noise in Channel 3 makes it difficult to use data from this channel in climatological studies”). Some  
54 noise filtering procedures were developed [2,3] and had some success but no method evolved into  
55 any integral and vital part of the standard AVHRR pre-processing software packages which are now  
56 widely used to prepare data for climate monitoring purposes. Thus, it is still up to each data  
57 producer to deal with this problem and take the necessary precautions.

58  
59 One reason for why the problem has been largely ignored (or possibly dealt with by more  
60 simple lowpass filtering methods) has been its intermittent appearance among the early satellites in  
61 the NOAA satellite series. For some satellites (e.g. NOAA-7, NOAA-9 and NOAA-12) and for some  
62 periods of the satellite lifetime the problem has been significant but for others (e.g. NOAA-11 and  
63 NOAA-14) the problem has been less pronounced. After introduction of the third version of the  
64 AVHRR sensor (AVHRR/3, first appearing on satellite NOAA-15 launched in 1998) the core  
65 interference problem was finally solved technically which further limited the interest in the problem.  
66 This evolution of channel 3b sensor performance is nicely summarized in [4] (Table 1). However, the  
67 increasing interest in creating climate data records based on AVHRR data, which is now the longest  
68 available multispectral image data record available (with data since 1978), means that this issue  
69 arises again and must be dealt with.

70  
71 This paper presents a method for filtering channel 3b noise based on a dynamic filtering  
72 approach utilizing the recorded time variability of the noise and the dependence on the scene  
73 temperatures. The method has primarily been used in the preparation phase of one particular  
74 climate data record; the CLARA-A2 data record [5]. The acronym stands for CM SAF (Climate  
75 Monitoring Satellite Application Facility, [www.cmsaf.eu](http://www.cmsaf.eu)) cLoud, Albedo and surface RAdiation  
76 dataset from AVHRR data – Second Edition. CLARA-A2 covers a 34-year period (1982-2015) and we  
77 will demonstrate the impact with and without a channel 3b noise filter on the resulting cloud  
78 products.

79  
80 Section 2 will introduce the problem of channel 3b noise ~~more in greater~~ depth ~~regarding with~~  
81 regard to the cloud screening process of AVHRR imagery with examples given for one of the early  
82 polar orbiting NOAA satellites. The method for reducing the impact of the noise is presented in  
83 Section 3 and full-scale results based on the entire 34-year data record are presented in Section 4. The  
84 impact and validity of the filtering procedure for the CLARA-A2 data record is discussed in Section  
85 5 with final conclusions given in Section 6.

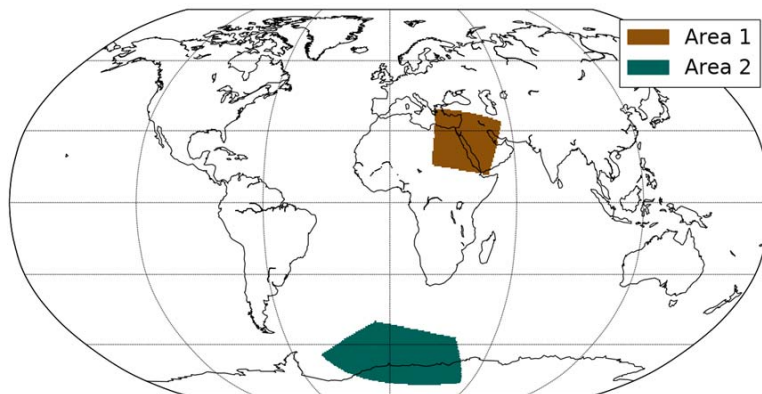
## 86 2. The importance of channel 3b noise for multispectral cloud screening of AVHRR data

87 To illustrate what the noise problem could really mean for cloud screening methods applied to  
88 AVHRR imagery, we present two examples in Figs 2 and 3 taken from one NOAA-7 orbit in Figures  
89 1 and 2 from 1<sup>st</sup> of January 1983 with the first scanline recorded at 00:07 UTC. We have selected two  
90 test areas, with positions displayed in Figure 1, where noise problems were found to be particularly  
91 serious. The figures show two portions of an Figs 2 and 3 are composed from AVHRR Global Area  
92 Coverage (GAC) orbit data in with a horizontal resolution of approximately 4 km. from 1<sup>st</sup> of January  
93 1983 with the first scanline recorded at 00:07 UTC. Figure 3 explains the orientation and land marks

Formaterat: Upphöjd

94 | ~~in the images as well as the used colour scale for the presented cloud type products.~~ These figures  
95 | are examples taken from a NOAA-7 period when the channel 3b noise for that satellite reached  
96 | remarkably high levels (see also Figure 4). The applied cloud processing method is the same as being  
97 | used for the generation of CLARA-A2 [5,6].

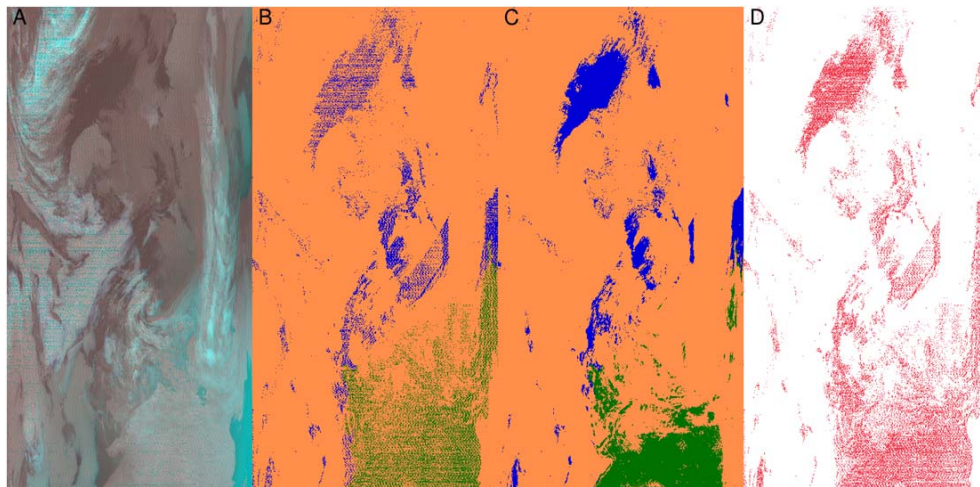
98 | The first example in Figure 2 (corresponding to Test area 2 in Figure 1) illustrates typical  
99 | problematic conditions for night-time and twilight AVHRR imagery over a region near Antarctica  
100 | where the visible part of Antarctica has very cold surface temperatures. The typical herringbone  
101 | pattern can be seen everywhere in Figure 2+Aa and most pronounced for thick midlevel clouds and  
102 | other cold surfaces (e.g. Antarctic surfaces in the lower portion of Figure 2+Aa). The effect on the  
103 | resulting cloud typing mask image is illustrated in Figure 2+Bb (~~where the associated colour legend~~  
104 | ~~for cloud types is given in Figure 3e~~). The most striking false features in the cloud type mask  
105 | product is the noisy striped pattern seen over presumably cloud free areas over ocean (upper part of image)  
106 | and over the Antarctic surface (at the bottom of the image). For most other parts the cloud screening  
107 | seems to work satisfactorily indicating that ~~other~~ cloud tests other than the ones related to channel  
108 | 3b are safely able to detect most clouds. Thus, we find most problems over cloud-free parts of the  
109 | image where other cloud tests are not indicating clouds.



110

111 | **Figure 1.** ~~Channel 3b noise effects in a portion of an AVHRR GAC orbit near Antarctica (see Figure 3~~  
112 | ~~for more location details) from 1<sup>st</sup> of January 1983 (near 00 UTC). (a) Colour composite image~~  
113 | ~~based~~ Test areas chosen for visualization of problematic channel 3b noise conditions in one selected  
114 | NOAA-7 AVHRR GAC orbit from 1<sup>st</sup> of January 1983 (see Figs 2 and 3).

Formaterat: Upphöjd



115

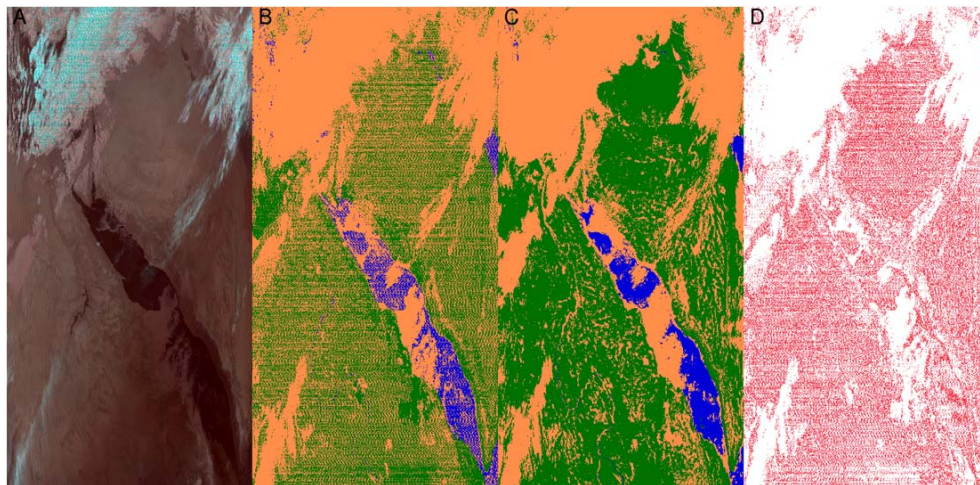
116 **Figure 21.** Channel 3b noise effects in a portion of an AVHRR GAC orbit near Antarctica (see Figure  
 117 3 for more location details Test Area 2 in Figure 1) from 1<sup>st</sup> of January 1983 (near 00 UTC). (Aa)  
 118 Colour composite image based on brightness temperatures of the three AVHRR infrared channels  
 119 3b, 4 and 5 at 3.7, 11 and 12 microns, respectively; (Bb) Cloud type-mask product for the same image  
 120 (orange is cloudy, blue/black is cloudfree water and green is land (including snow covered land); pink  
 121 cloudfree snow/ice—see Figure 3c for detailed colour legend).-(Cc) Cloud type-mask product after  
 122 using the channel 3b noise filter; (D) Difference plot where red indicates either removal or adding of  
 123 clouds.-

124 Figure 32 shows another portion of the same AVHRR GAC orbit over the Arabian peninsula and  
 125 adjacent regions (Test area 1 in Figure 1), now observed under exclusively night-time conditions.  
 126 The herringbone pattern is not as easily seen in Figure 32Aa as in the previous Figure 21Aa but the  
 127 effects on the cloud type product in Figure 32Bb is immenseare substantial. The noisy pattern of false  
 128 clouds almost dominates the scene. The two examples shown here are indeed extreme cases selected  
 129 from conditions with very high levels of channel 3b noise. Nevertheless, they clearly illustrate the  
 130 vulnerability of the cloud screening process to these unwanted fluctuations and perturbations of the  
 131 infrared radiances and brightness temperatures.

132 To understand the seemingly variable sensitivity toThe two examples in Figs 2 and 3 indicate that  
 133 the impact of -channel 3b noise in the cloud screening process varies depending on the situation.  
 134 (i.e. For example, it is not always the areas with most evident and-visible noise patterns in the  
 135 radiance images (i.e., Figs 2A and 3A) that creates the largest changes of the cloud mask product.  
 136 cloud typing errors); To understand this, we need to recall some of the most essential principles for  
 137 the cloud screening process. As elaborated on-in detail in [7,8], the 3.7 micron channel offers a very  
 138 important complementary capability for cloud screening compared to the more traditional visible  
 139 and infrared channels. For visible channels, clouds are generally brighter than the surface and the  
 140 same is true for infrared channels provided that the signal is inverted so that the coldest targets are  
 141 shown as bright targets and vice versa. But this method will fail for most clouds located over snow  
 142 surfaces or for low (warm) clouds over bright land surfaces (e.g. deserts). Also thin cirrus clouds  
 143 over relatively cold and bright surfaces might escape detection by use of traditional visible/infrared  
 144 methods. But since water clouds as opposed to ice clouds have a reflecting capability higher  
 145 reflectance in the 3.7 micron channel while bright surfaces than cloud-free surfaces (especially snow  
 146 cover), reflect much less this channel is particularly useful as a complement to the visible and  
 147 infrared cloud tests. These clouds' ability to reflect sunlight also means that they will not act as  
 148 perfect blackbodies at night. Thus, by comparing their brightness temperatures to the measurements  
 149 at longer infrared wavelengths at (where they act more like blackbodies), clouds can be detected also

150 at night even if cloud temperatures are close to the surface temperatures. At the same time, cloud  
 151 transmissivities for thin cirrus clouds are larger at 3.7 microns than at longer wavelengths. This  
 152 means that if studying e.g. the brightness temperature difference between the channel at 3.7 microns  
 153 and the channel at 12 microns at night we get a positive difference for thin cirrus clouds and a  
 154 negative difference for thick water clouds. The cloud-free surface generally does not show these  
 155 differences at night, although some compensations or corrections have to be applied over desertic  
 156 regions where surface emissivities may vary (in CLARA-A2 this is done using MODIS-derived  
 157 surface emissivity climatologies). Because of this, AVHRR channel 3b is quite important in the cloud  
 158 screening process. It also follows that, since this channel is also central for the determination of other  
 159 cloud properties (like cloud phase and cloud droplet characteristics), these noise problems will also  
 160 increase the uncertainty in the retrieval of other cloud products other than the cloud mask.

161 From this background it follows that if periodically and spatially varying noise is added to the  
 162 channel 3b measurement, the night-time and twilight cloud separability in infrared AVHRR channel  
 163 data could be seriously affected. If the noise has a large amplitude (as illustrated in Figures 24 and  
 164 32) it creates artificial brightness temperature variations in channel 3b and consequently also in all  
 165 brightness temperature difference features involving this channel. In the worst case, a wave-like  
 166 pattern of alternating false low cloud types and thin cirrus clouds may appear in the cloud typing  
 167 process despite truly and completely cloud-free conditions. This is exactly what is illustrated in  
 168 Figure 32Bb. Without the extra noise in the measurement we would not have any remarkable  
 169 brightness temperature differences between measurements in the 3.7 micron and the 12 micron  
 170 channels and we would have achieved completely cloud free conditions in the cloud type-mask  
 171 product. But due to the strong noise with a high amplitude the result is instead turned into a  
 172 dominantly but falsely cloudy state. Bad conditions can also occur in twilight conditions (here  
 173 defined as the solar zenith interval 80-95 degrees - often associated with the time of the daily  
 174 minimum of the surface temperature) but for higher sun elevations the reflected component  
 175 measured in the 3.7 micron channel eventually dominates over the emitted one and the problems  
 176 diminish.



177

178 **Figure 32.** Channel 3b noise effects in a portion of an AVHRR GAC orbit over Egypt and the Arabian  
 179 peninsula (see Figure 3b for more location details Test Area 1 in Figure 1) from 1<sup>st</sup> of January 1983  
 180 (near 00 UTC). (A) Colour composite image based on brightness temperatures of the three AVHRR  
 181 infrared channels 3b, 4 and 5 at 3.7, 11 and 12 microns, respectively; (B) Cloud type-mask product  
 182 for the same image (using the same colour table as in Figure 2 B and 2C), using a simplified colour  
 183 legend where thick clouds are orange, thin clouds grey, cloud-free land green and cloud-free sea

184 | ~~blue~~. (Ce) Cloud ~~type-mask~~ product after using the channel 3b noise filter: ~~-(D) Difference plot~~  
185 | ~~where red indicates either removal or adding of clouds.~~

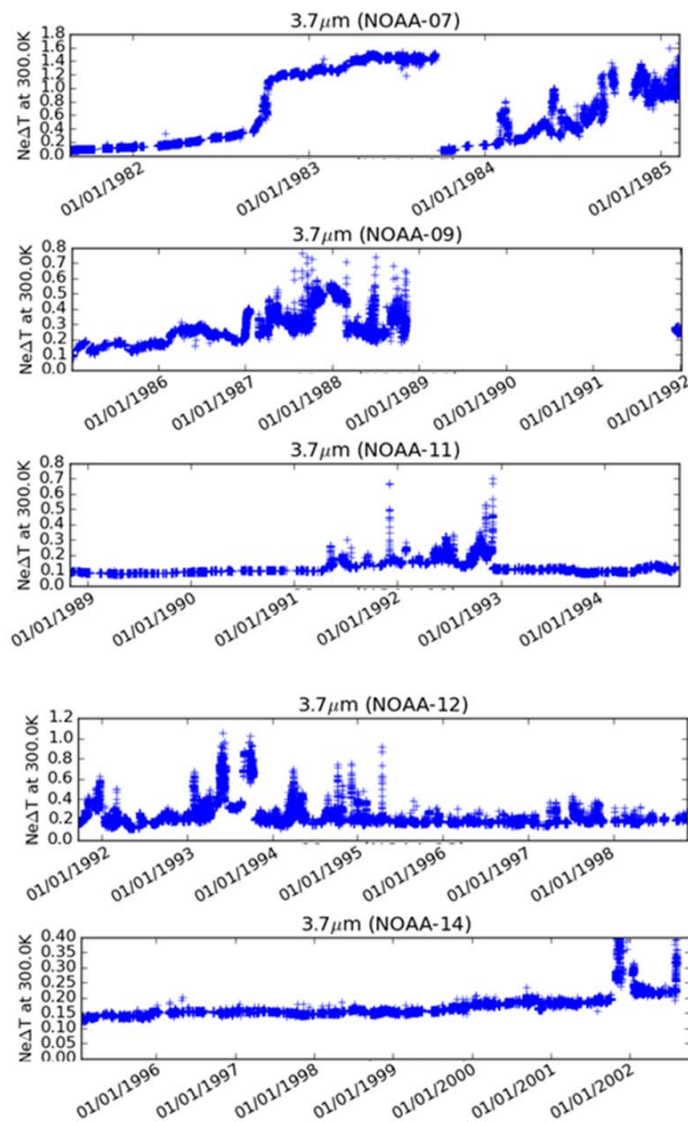
186

187

#### 188 4. Development of a dynamic channel 3b noise filter

189 The complex behavior of the channel 3b noise means that no standard lowpass filters with fixed size  
190 can be used to remove it, simply because the noise pattern varies in time and space in AVHRR  
191 imagery. One particularly difficult feature is that for higher noise levels ~~also~~ the pattern of the noise  
192 changes, often yielding ~~a larger scale of the noise~~ noise with a larger spatial scale (i.e., longer spatial  
193 wavelengths). Even though more complex methods have been attempted on high resolution  
194 AVHRR imagery [2,3], their applicability to a large data record of historic and coarse resolution  
195 AVHRR GAC orbits have not yet been demonstrated.

196 The noise filtering method developed in the preparation phase of the CLARA-A2 data record should  
197 be seen as a data rescue action rather than as a data recovery action. Thus, we want to retrieve as  
198 much as possible of the true Earth observation signal without risking destroying true signals (also  
199 pointed out specifically in [2]). More clearly, the filter must only be used when needed and not in  
200 noise-free or close to noise-free situations. If applying it in the latter situation, the true signal could  
201 be altered in a way that fine resolution details are lost, i.e., true brightness temperature differences at  
202 the finest scales might be removed. Thus, the use of the filter has to be tightly linked to the actual  
203 level of the channel 3b noise for each AVHRR sensor. The natural choice for linking the filter to noise  
204 levels is to make use of measured space count variability of the sensor onboard the satellite. For each  
205 scan of the sensor there is a measurement into deep space that is used as the lower calibration  
206 reference. The space count would be a stable value in undisturbed conditions but this measurement  
207 is also affected by the external interference disturbance onboard the space platform causing the  
208 channel 3b noise problem. Thus, a measurement of the variance of the space count would be a good  
209 measure of the channel 3b noise level. Figure 4 gives the noise equivalent delta temperature  
210 ( $Ne\Delta T$ ) derived from the space view measurements for all AVHRR sensors on satellites NOAA-7,  
211 NOAA-9, NOAA-11, NOAA-12 and NOAA-14 (i.e., the satellites carrying the AVHRR/2 sensor,  
212 remembering that the CLARA-A2 data record only uses data from the AVHRR/2 and AVHRR/3  
213 sensors). The noise is first estimated from the raw counts observed when looking at space and is  
214 derived from data aggregated over a complete orbit. Here we note that due to the electronic  
215 clamping performed on-board the AVHRR there is no variation in the mean value of the space view  
216 counts. The derived counts noise is then converted into noise in radiance space using the AVHRR  
217 calibration equation ~~using with~~ the average instrument gain determined over the given orbit. The  
218 radiance noise is then converted into the  $Ne\Delta T$  using the Planck function at a fixed scene  
219 brightness temperature, in this case 300\_K. We can, in particular, see the problematic behavior of ~~the~~  
220 channel 3b for satellites NOAA-7, NOAA-9 and NOAA-12 while the other satellites show less of a  
221 problem, with high noise levels occurring only sporadically. Notice also that for NOAA-7 the high  
222 noise levels were reduced back to more normal levels in autumn 1983 by specific satellite operations  
223 but this lasted only for a couple of months until noise levels started to increase again.



224

225 **Figure 4.** Channel 3b noise, expressed as noise equivalent temperature variation ( $Ne\Delta T$ ) at the 300 K  
 226 level, during the lifetime of satellites NOAA-7, NOAA-9, NOAA-11, NOAA-12 and NOAA-14.

227 In addition to a dependency on actual noise levels, we also need to deal with the fact that noise levels  
 228 will be more serious for cold image targets than for warm targets. ~~This which~~ is a consequence of the  
 229 non-linear transfer of original counts and radiances into brightness temperatures using the inverse  
 230 Planck function. Thus, we need to apply a filter that is dynamic in its size and influence area, and  
 231 which is a function of channel 3b noise levels and the actual scene temperature.

232 Several types of filters were tested, including the Wiener filter proposed in [2]. However, the final  
 233 choice was to use a Median filter, ~~which is a filter that~~ replaces the central pixel value in the filter  
 234 kernel of size N with the median value in the kernel. The main advantage ~~with of~~ the Median filter is  
 235 the treatment in areas where 'no data'-pixels exist, ~~i.e., pixels where measurements are lacking (e.g.,~~

236 ~~due to sensor registration problems or scan motor issues~~) which ~~also rather~~ frequently occurs in  
 237 historic AVHRR data. The median filter ~~will not attempt any interpolation or altering of values for~~  
 238 ~~such pixels but just leaves the pixel unchanged.~~ may change a pixel value from Nodata to the median  
 239 of the surrounding pixels radiance values and vice versa but as long as we have valid radiances in  
 240 other AVHRR channels for this pixel, the results are not changed significantly. Most important is  
 241 that if we also have Nodata in all other channels the impact will be zero, i.e., this will result in  
 242 Nodata in the cloud product regardless of having performed filtering or not. The median filter also  
 243 preserves cloud edges better than mean filters. The filter was also found to be about three times  
 244 faster than the Wiener filter which is an important aspect when processing very large datasets.

245 The ~~finally applied~~ methodology can be summarized as follows:

- 246 1. A Median filter is applied with dynamic kernel size as a function of channel 3b noise levels.
- 247 ~~2. The kernel size is varied between 3x3 GAC pixels for low noise levels and 13x13 GAC~~  
 248 ~~pixels for the highest noise levels. The size of the used circular kernel is varied from radius~~  
 249 ~~of 2 GAC pixels for low noise levels (up to 0.1) to a radius of 7 GAC pixels for the highest~~  
 250 ~~noise levels (above 1.25). Radius of 2 means that in total 13 pixels including the considered~~  
 251 ~~central pixel are included. For noise levels between 0.1 and 1.25 the radius is linearly~~  
 252 ~~interpolated between the two and rounded down to nearest integer.~~
- 253 ~~2-3. A slightly modified definition of the noise level  $n_l$  was used compared to what is shown in~~  
 254 ~~Figure 4. Instead of using the standard deviation of the space count we use the standard~~  
 255 ~~deviation of the internal black body count. Both quantities are highly correlated but the~~  
 256 ~~black body count gives a slightly smoother dependency curve which better resemble the~~  
 257 ~~measurement variability of Earth view measurements. After applying a constant scale~~  
 258 ~~factor,  $n_l$  is adjusted to gives values which approximately match the range of values in~~  
 259 ~~Figure 4.~~
- 260 ~~3-4. A post-processing restoral approach is applied in addition to reduce the effect of~~  
 261 ~~erroneously removing pixel-scale true clouds over warm surfaces.~~

262 The third step here is a way of introducing a scene temperature dependency on the filtering method.  
 263 If not applying any restoral method, small-scale features (e.g. cumulus clouds or small holes in cloud  
 264 decks) that are correctly depicted in the warmer parts of AVHRR scenes (i.e., not produced by noise)  
 265 might risk to be lost after filtering. The restoral method checks the temperature correction  $\Delta T$   $\Delta T$  for  
 266 each pixel and judges if this is a reasonable correction or not by checking the pixel temperatures. If  
 267 the correction is not found to be reasonable (i.e., exceeding a maximum  $\Delta T_{MAX}$   $\Delta T_{MAX}$  range), the  
 268 value is restored back to its original channel 3b brightness temperature.

269 An optimal determination of the parameter  $\Delta T_{MAX}$   $\Delta T_{MAX}$  is crucial for the restoral method to be  
 270 efficient. ~~Most important here is that  $\Delta T_{MAX}$~~  it should be linked to the actual noise levels in radiance space  
 271 rather than to brightness temperatures to avoid too strong non-linear effects due to the dependency  
 272 on the Planck Function. We have chosen to formulate  $\Delta T_{MAX}$   $\Delta T_{MAX}$  using a reference temperature at  
 273 270 K and with a linear dependency on the noise level  $n_l$ . ~~More clearly, we~~ We first define that at a  
 274 temperature 270 K plus a temperature deviation  $\Delta T_{MAX}$   $\Delta T_{MAX1}$  the maximum allowed temperature  
 275 difference  $\Delta T_{MAX}$   $\Delta T_{MAX1}$  should follow the relation given by

$$276 \quad \Delta T_{MAX1} (270 + \Delta T_{MAX1}) = 15n_l \quad (1)$$

277 Via the Planck Function  ~~$B_1(T)$~~   $B_1(T)$  we can then calculate the corresponding radiance difference  
 278  ~~$\Delta R_{MAX}$~~   $\Delta R_{MAX}$  (resulting for a temperature  $\Delta T_{MAX}$   $\Delta T_{MAX1}$  warmer than the studied temperature) by

$$\Delta R_{MAX} = B_{\lambda=3.7 \mu m}(270 + 2\Delta T_{MAX1}) - B_{\lambda=3.7 \mu m}(270 + \Delta T_{MAX1}) \quad (2)$$

We will now use this radiance difference and keep it fixed to recalculate the corresponding  $\Delta T_{MAX}(T)$  to be used for all other temperatures than 270 K in the relation

282

$$\Delta T_{MAX}(T) = B_{\lambda=3.7 \mu m}^{-1} [B_{\lambda=3.7 \mu m}(T) + \Delta R_{MAX}] - T \quad (3)$$

In this way we get a more realistic calculation of the impact of the noise ~~compared to than~~ if we had formulated this entirely in brightness temperature space. The reason is that the noise ~~should be seen as is a~~ constant addition to the true radiance measured by the sensor regardless of its actual value (thus, without temperature dependence).

Table 1 describes the resulting  $\Delta T_{MAX}(T)$  values for some selected temperatures for the restoral method. Results are ~~here~~ given ~~here~~ for one low noise level category and one high noise level category. We notice the strong dependency on the noise level so that the allowed temperature difference after filtering is higher for cases with very high noise levels. Notice, however, that as an extra precaution ~~measure~~ we always perform filtering if both the original and filtered channel 3b brightness temperatures are colder than a certain value (here 263 K), acknowledging the fact that for cold temperatures the impact of channel 3b noise is likely to be very high and further augmented by poor radiometric resolution effects. Thus, our restoral method will then be less justifiable or relevant and should therefore be discarded.

A problem with this method is that, if just relying on channel 3b brightness temperatures for the determination of  $T$  and  $\Delta T_{MAX}(T)$ , the noise itself might have altered the scene temperature so much that it is not truly representative any more. Thus, in order to not be too sensitive to the noise effect in very cold situations, we have applied a combined use of 3.7 micron and 11 micron brightness temperatures as follows:

1. At night (defined as situations with less than 1 % reflectivity measured in AVHRR channel 1) use 11 micron brightness temperatures as the reference when calculating  $\Delta T_{MAX}(T)$ .
2. During daytime, use the maximum of the original and the filtered 3.7 micron brightness temperatures as the reference when calculating  $\Delta T_{MAX}(T)$ .

**Table 1.** Example of maximum allowed temperature differences ( $\Delta T$ ) after Median filtering for two different noise level categories and as a function of some selected scene temperatures (column 1). Notice that the applied method uses a finer temperature resolution of the tabulated values than presented here).

\* If both the filtered and original 3.7 micron brightness temperatures are colder than 263 K, no restoral is applied at all.

Temperature (K)	$\Delta T_{MAX}(T)$ (K) Noise level 0.1	$\Delta T_{MAX}(T)$ (K) Noise level 1.25
220	15.8*	74.0*
230	10.3*	64.3*
240	6.4*	54.8*
250	4.0*	45.9*
260	2.5*	37.5*
270	1.6	30.0

280	1.0	23.5
290	0.7	18.1
300	0.5	13.8
310	0.3	10.5
320	0.3	8.0

313

314

### 315 3. Results

#### 316 3.1. Impact on individual GAC scenes

317 Two examples of how filtered products compare to unfiltered products are given in Figures [24Ce](#)  
318 and [32Ce](#).

319 Visual inspection indicates a very ~~satisfying~~ satisfactory performance of the filtering in Figure [24Ce](#).  
320 Obviously cloud-free regions over ice-free ocean are now restored completely, ~~(i.e.,~~ getting rid of  
321 the noisy pattern of false clouds). ~~Also,~~ The visible part of Antarctica in the lower part of the GAC  
322 scene is now described more realistically, ~~revealing~~ revealing large cloud-free areas over the Antarctic  
323 continent.

324 The other example in Figure [32Ce](#) shows a less efficient case where the filtering is only capable of  
325 removing some of the false clouds. It shows that, in some situations, very serious noise patterns  
326 create conditions which are not possible to restore completely and only some reductions can be  
327 achieved. In particular, in regions where false clouds dominate, a median filter (or any other of the  
328 tested filters) cannot recover the original signal very well.

#### 329 3.2. Regional differences in monthly climatologies

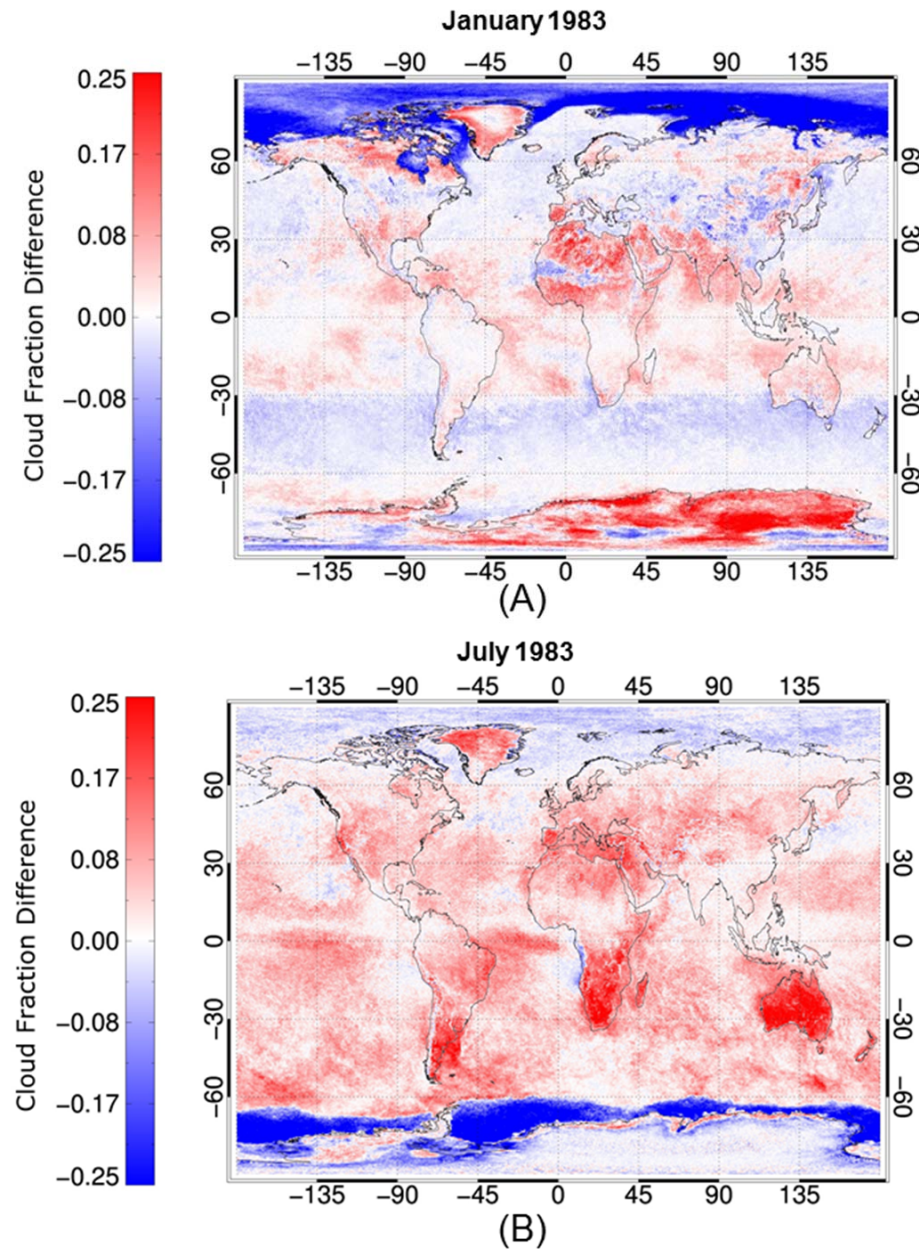
330 To study the full impact of the filtering process, one has to look at the impact on real climatologies  
331 based on the aggregation of a large number of GAC orbits. This cannot ~~be done~~ easily ~~be done~~ by  
332 simple prototyping efforts because of the need ~~of for~~ a very extensive processing of data. However,  
333 we will ~~here~~ take advantage of the fact that two complete but slightly different versions of the  
334 CLARA-A2 data record were ~~actually~~ produced. This is explained by the fact that the first  
335 reprocessing effort had to be repeated after discovering some minor technical problems affecting a  
336 small part of the GAC dataset and also because of a minor arithmetic error in the calculation of  
337 monthly climatologies. This reprocessing offered a chance ~~of to~~ introducing the new noise filtering  
338 procedure and to study the full impact of it over the entire 34 year period. Thus, by comparing the  
339 two versions of the data record and by considering the other changes made to the processing it is  
340 possible to study the sole impact of the channel 3b noise filtering.

341 In summary, the following changes were introduced in the second and final reprocessed version of  
342 the CLARA-A2 data record:

- 343 1. Updated method of removing overlap between consecutive GAC orbits.
- 344 2. Removal of an incorrect ~~arithmeti~~ rounding error in the calculation of monthly means.
- 345 3. Blacklisting of a number of NOAA satellite orbits in the period 2000-2004 due to scan motor  
346 problems.

## 347 4. Introduction of the channel 3b noise filter.

348 The first item regarding the orbit overlap treatment had negligible impact on final climatologies  
349 since it only affected a small fraction of GAC orbits and for every affected orbit only impacted a few  
350 scan lines (out of more than 12 000 lines) per GAC orbit. The second item had a much larger effect on  
351 results since it ~~basically~~ meant that values were rounded to the nearest lower integer value in the  
352 first CLARA-A2 processing effort. In the case of cloud fraction it meant that results were biased low  
353 with a value between 0-1 % in absolute values. This feature becomes quite noticeable for very cloudy  
354 regions where overcast gridboxes have been systematically given a cloud fraction value of 99%  
355 instead of 100%. For any other region, the cloud fraction is distributed over a larger value range, and  
356 the difference will be smaller but still negative (i.e., underestimated). However, in practice the  
357 correction would be close to 1 % in global averages since the overcast situations dominate over  
358 fractionally cloudy or cloud free cases. But since this correction would be valid and relatively stable  
359 over the entire data record it can be adequately accounted for in this particular study. The third item  
360 is actually mostly irrelevant for the channel 3b noise study since this affected only a few months of  
361 data from NOAA-14 at the end of its lifetime. Thus, if restricting the study to the period 1982-1999,  
362 we would see the full effect of channel 3b noise filtering provided that we also take into account the  
363 ~1 % increase in cloud fraction due to the correction of the rounding error.



364

365 **Figure 5.** Cloud fraction difference for January 1983 (A) and July 1983 (B) for the CLARA-A2  
 366 climatology after applying channel 3b noise filter and a rounding error correction (approximately -  
 367 0.01 everywhere). Observe that the figure shows unfiltered minus filtered CLARA-A2 results, i.e.,  
 368 red colours indicating reduction after filtering and blue colours an increase after filtering. The  
 369 globally averaged cloud fraction difference in January 1983 was +0.4 % and in July 1983 4.2 %.

370 Figures 5 and 6 shows the impact of the channel 3b noise filtering and the rounding error correction  
 371 for the mean CLARA-A2 cloud fraction of the months of January and July 1983 from the NOAA-7

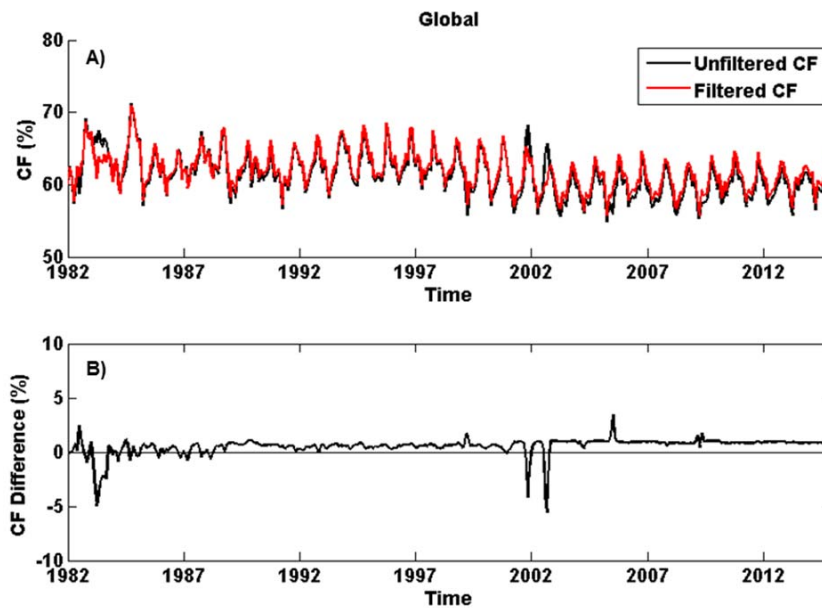
372 satellite. In both these months the channel 3b noise levels were very high (see Figure 4). Thus, the  
373 figures illustrate more or less the maximum effects that were encountered during channel 3b noise  
374 filtering.

375 We conclude that the effect of the filtering is much larger than the effect of the rounding error. In  
376 fact, filtering is able to change monthly mean cloud cover by more than 25 % in some regions  
377 compared to the maximum change of 1 % from the rounding error. For example, Australia stands  
378 out in particular in the results for July 1983 (Figure 5B6) where reductions larger than 25 % can be  
379 seen almost over the entire continent. Other regions with large reductions are southern Africa and  
380 the southern part of South America in July 1983 and parts of Antarctica in January 1983. The filter  
381 obviously remove clouds over large areas (red parts ~~of in Figures 5 and 6~~) but ~~surprisingly~~, it also  
382 leads to large increases in cloudiness in some regions. The increases are most pronounced over sea  
383 ice regions during polar winter seasons. This is explained by the specific cloud mask thresholding  
384 sequence ~~applied differences~~ over land and sea in very cold situations at night. Previously (with no  
385 filter applied), conditions with high noise levels would allow temperatures to vary wildly in channel  
386 3b in very cold situations. Since this was known to seriously impact brightness temperature tests,  
387 those tests were simply turned off when temperatures fell below a threshold (230 K). However, the  
388 filtering process now causes a large number of those pixels to register as warmer than 230 K, and be  
389 analyzed using the brightness temperature tests. This leads to a labelling of more cloudy pixels than  
390 before. lead to that a larger fraction of those pixels (now becoming warmer than 230 K) were actually  
391 analysed using the brightness temperature tests (i.e., the median filter did not allow previous large-  
392 variations) and this lead to a labelling of more cloudy pixels than before. Further, many of these tests  
393 ~~also~~ have also an additional condition that the variance in channel 3b ~~7~~ should not be too high. Large  
394 variance over sea ice indicates either noise in channel 3.7 or ice cracks. The filtering procedure  
395 generally reduced this variance over sea ice regions which also leads to the detection of more  
396 clouds, this increase after applying filtering became particularly large. These circumstances lead to  
397 an apparent asymmetry in the resulting changes over the two polar regions. However, if just  
398 separating the effects over sea ice and land portions, respectively, the effects appear to be rather  
399 similar over both polar regions.-

400

### 401 3.3. Contribution to 34-year trend in cloudiness

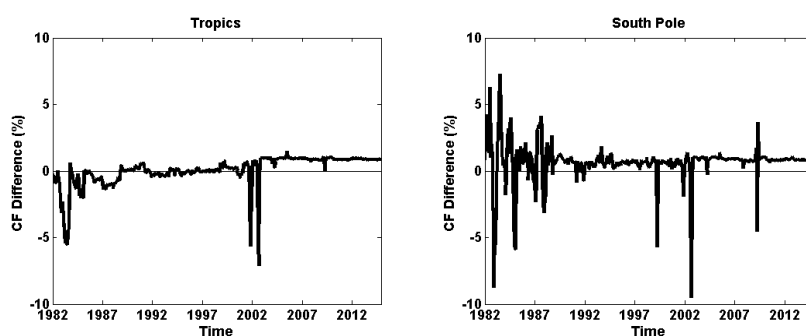
402 ~~Finally, let's study how the filtering affected global cloud conditions throughout the 34 year~~  
403 ~~CLARA-A2 time period.~~ Figure 6Z shows the globally averaged cloud cover for the two CLARA-A2  
404 versions and a difference plot. ~~First, observe that in~~ in the period 2000-2003 a significant fraction of  
405 GAC orbits were removed which caused ~~rather~~ large changes in results. ~~But after 2003 we~~ After 2003,  
406 ~~there is notice~~ an almost constant change of just below 1 % cloud cover except for some spikes  
407 caused by the removal of some additional erroneous GAC orbits. This is the impact of correcting for  
408 the rounding error. In the period 1982-1999 we should only see the combined effect of the corrected  
409 rounding error and the introduction of the median filter to channel 3b brightness temperatures. It is  
410 clear that, since the rounding effect should be ~~rather~~ approximately constant over the years (varying  
411 marginally with the global mean cloud cover), the filtering procedure generally leads to reduced  
412 cloudiness (i.e., the difference is generally smaller than 1 %). This reduction is largest in the  
413 beginning of the period (1982-1988 with the NOAA-7 and NOAA-9 satellites) with an extreme  
414 negative peak in July 1983 (corresponding to the situation illustrated in Figure 5B6). The variability  
415 in the impact of the filtering effect is also largest in this early period.



416

417 **Figure 67.** A) Global mean cloud fraction difference (% cloud cover) for the entire time period  
 418 1982-2015 between for the final version of CLARA-A2 and the original CLARA-A2 version. B) Mean  
 419 cloud fraction difference between filtered and unfiltered results. The impact of channel 3b filtering is  
 420 visible in the period 1982-1999 (see text).

421 As indicated by Figures 5 and 6, the regional impact might be quite different from the impact given  
 422 by the global mean figures in Figure 67. This is further exemplified in Figure 78, showing the impact  
 423 (i.e., difference after filtering) for the tropical region and the south pole region. It is clear that for  
 424 lower latitudes the effect of filtering is mainly the removal of (presumably) false clouds while at  
 425 higher latitudes the effect alternates between mainly removing clouds in the polar summer and  
 426 adding clouds in the polar winter.



427

428 **Figure 78.** Mean cloud fraction difference (% cloud cover) in the tropical region (Tropics) and the  
 429 South Pole region (Spole) for the entire time period 1982-2015 between the final version of  
 430 CLARA-A2 and the original CLARA-A2 version. The impact of channel 3b filtering is visible in the  
 431 period 1982-1999 (see text).

432

433

434 **4. Discussion**

435 Results in Section 3 imply that AVHRR channel 3b noise is capable of degrading cloud climate  
436 data records considerably, especially during periods of high noise levels. If assuming that  
437 corrections are reasonable, results show that ignoring noise effects might contribute to an overall  
438 decreasing trend of about 1-2 % per decade in cloud cover over the period (with largest  
439 overestimations in the beginning of the period). In addition to this, noise will increase the variability  
440 of climate relevant parameters in an unrealistic way. For the CLARA-A2 data record specifically, this  
441 appeared to be most serious for the polar regions where noise effects caused seasonally varying and  
442 opposed effects.

443  
444 The artificial trend might be specific for CLARA-A2 due to the heavy use of cloud tests based  
445 on the brightness temperature differences between channel 3b and the other infrared channels.  
446 However, other data records making heavy use of AVHRR channel 3b data (e.g. PATMOS-x [9] and  
447 ISCPP [10]) are also likely to be influenced negatively by AVHRR channel 3b noise.

448  
449 No filtering method will probably ever be capable of completely recovering the original  
450 AVHRR noise free measurement, especially not in situations with very high noise levels that  
451 completely dominate the measurement. But the use of dynamically varying filters has some success  
452 even ~~at~~ with these very problematic conditions as demonstrated in this study. Thus, applying filters  
453 will definitely have some data rescuing value. As such, the method is probably only applicable to  
454 AVHRR data because of the very specific origin and character of the noise caused by interference  
455 with other systems onboard the NOAA satellite platform.

456  
457 Despite the seemingly modest impact of the noise on global trends, we cannot ignore the fact  
458 that accuracy requirements of measurements to be used for climate change studies are very strict  
459 and demanding [11]. In that perspective, the noise problem has to be tackled appropriately together  
460 with other calibration and navigation issues of AVHRR GAC data.

461  
462 The results presented in this paper should be seen as a first more extensive and systematic effort  
463 of handling the channel 3b noise problem in the production of an AVHRR GAC based climate data  
464 record. The method was not only used for CLARA-A2 generation but it has also been used in a  
465 project for generating an AVHRR-heritage cloud data record [12] of the ESA Climate Change  
466 Initiative (CCI) programme [13]. The latter project aims at studying the specific essential climate  
467 variable (ECV) denoted “cloud properties” and the project is formally named ESA-CLOUD-CCI [14].  
468 The filtering functionality will also be added to the general AVHRR calibration and pre-processing  
469 software package PyGAC [15].

470  
471 Future improvements of the methodology are possible. Especially, the filtering procedure  
472 should preferably be carried out in radiance space rather than in brightness temperature space in  
473 order to avoid the strongly non-linear effects (in particular affecting cold scene temperatures)  
474 resulting when applying the inverse Planck function. However, this requires some improved  
475 flexibility of the currently used state of the art calibration and pre-processing tools. A first  
476 demonstration of such a radiance-based filtering approach applied to the entire AVHRR GAC  
477 dataset has recently been made by NASA [17]. This method doesn't use pre-existing knowledge of  
478 temporally varying noise characteristics but is instead based on a segmentation of individual GAC  
479 orbits into smaller segments where a Fast Fourier transform analysis and filtering can be made. This  
480 method is very interesting and results will be studied and compared to the current method in the  
481 near future. The most interesting aspect of these future studies of the two methods will be to check  
482 the balance between the removal of truly artificial noise features and the unwanted removal of small  
483 scale true features in the filtered AVHRR scenes.

484

485 | Finally, improved descriptions of noise and uncertainty characteristics, as well as a  
486 considerably upgraded infrared AVHRR calibration methodology are foreseen as important  
487 outcomes of the European Union Horizon 2020 project Fidelity and uncertainty in climate data  
488 records from Earth Observations (FIDUCEO, [16]). This will contribute to better means of handling  
489 radiance noise problems in fundamental climate data records (FCDR) such as the AVHRR GAC data  
490 record.

491

492

## 493 5. Conclusions

494 A method for reducing the impact of noise in the 3.7 micron spectral channel in climate data  
495 records derived from coarse resolution (5 km) global measurements from AVHRR data has been  
496 presented.

497 The impact of the noise was demonstrated for two selected cases from the NOAA-7 satellite in a  
498 period when noise levels were extremely high. Based on some fundamental characteristics of the  
499 noise, a dynamic size-varying median filter was suggested to be operated and guided by measured  
500 noise levels and being dependent on scene temperatures for individual AVHRR sensors. The impact  
501 of applying the noise filter was demonstrated for two selected monthly cloud climatologies as well  
502 as for the entire data record from 1982 to 2015. Globally, the filter generally reduced cloud cover  
503 leading to the removal of a decreasing global trend of about 1-2 % per decade in the period  
504 1982-2001. However, the impact of the filter showed strong regional and seasonal dependencies. For  
505 low latitudes, cloud cover was generally reduced while for the polar regions corrections were  
506 alternating positive or negative depending on season (positive in polar winter, negative in polar  
507 summers). Thus, not only the global trend was affected but also the climate variability in different  
508 regions.

509 The method has been used in the preparation of the CLARA-A2 data record as well for  
510 preparing the corresponding AVHRR-based datasets produced in the ESA project  
511 ESA-CLOUD-CCI.

512 Future improvements of the methodology can be achieved if applying filters in radiance space  
513 instead of in brightness temperature space to avoid the non-linear dependence from the Planck  
514 function. Such an approach has recently been applied [17] and corresponding results will be  
515 compared with the results of the current method in the future. Also, improvements based on a better  
516 characterization of the noise are anticipated as an outcome of the EU Horizon 2020 project  
517 FIDUCEO.  
518

### 519 Author Contributions:

520 Nina Håkansson and Karl-Göran Karlsson conceived and designed the experiments and carried out  
521 the prototyping of the method; Jon Mittaz prepared and provided the AVHRR channel 3b noise  
522 information, Timo Hanschmann and Abhay Devasthale prepared and analysed the resulting  
523 climate data records; Karl-Göran Karlsson wrote the paper.

524

### 525 Conflicts of Interest:

526 The authors declare no conflict of interest.

527

## 528 References

- 529 1. Cracknell, A.P. The Advanced Very High Resolution Radiometer, Taylor & Francis Ltd, UK, 1997.  
530 2. Simpson, J.J., Yhann, S.R. Reduction of noise in AVHRR channel 3 data with minimum distortion.  
531 *IEEE Transactions on Geoscience and Remote Sensing* **2002**, *32*, 315 – 328, DOI: 10.1109/36.295047.  
532 Available online: <http://ieeexplore.ieee.org/document/295047/?reload=true>  
533 3. Warren, D. AVHRR channel-3 noise and methods for its removal, *Int. J. Remote. Sens.*, **1989**, *10*,  
534 645-651, <http://dx.doi.org/10.1080/01431168908903905>  
535 4. Trishchenko, A. P., Fedosejevs, G., Li, Z. and Cihlar, J. Trends and uncertainties in thermal calibration  
536 of AVHRR radiometers onboard NOAA-9 to NOAA-16. *J. Geoph. Res.*, **2002**, *107*, D24, 4778,  
537 doi:10.1029/2002JD002353.  
538 5. Karlsson, K.-G., Anttila, K., Trentmann, J., Stengel, M., Meirink, J. F., Devasthale, A., Hanschmann, T.,  
539 Kothe, S., Jääskeläinen, E., Sedlar, J., Benas, N., van Zadelhoff, G.-J., Schlundt, C., Stein, D.,  
540 Finkensieper, S., Håkansson, N., and Hollmann, R. CLARA-A2: The second edition of the CM SAF

Formaterat: Indrag: Första raden: 0  
cm

- 541 cloud and radiation data record from 34 years of global AVHRR data, *Atmos. Chem. Phys. Discuss.*,  
542 doi:10.5194/acp-2016-935, in review, 2016.
- 543 6. Dybbroe, A., Thoss, A. and Karlsson, K.-G. NWC SAF AVHRR cloud detection and analysis using  
544 dynamic thresholds and radiative transfer modelling – Part I: Algorithm description, *J. Appl. Meteor.*,  
545 **2005**, 44, 39–54.
- 546 7. Karlsson, K.-G., Johansson, E. and Devasthale, A. Advancing the uncertainty characterisation of cloud  
547 masking in passive satellite imagery: Probabilistic formulations for NOAA AVHRR data, *Rem. Sens.*  
548 *Env.*, **2015**, 158, 126–139; doi:10.1016/j.rse.2014.10.028.
- 549 8. Musial, J. P., Hüsler, F., Sütterlin, M., Neuhaus, C., & Wunderle, S. Probabilistic approach to cloud  
550 and snow detection on Advanced Very High Resolution Radiometer (AVHRR) imagery. *Atm. Meas.*  
551 *Tech.*, 2014, 7, 799–822, <http://dx.doi.org/10.5194/amt-7-799-2014>.
- 552 9. Heidinger, A. K., Foster, M. J., Walther, A. & Zhao, Z. The Pathfinder Atmospheres Extended  
553 (PATMOS-x) AVHRR climate data set. *Bull. Amer. Met. Soc.* **2014**, 95, 909–922.
- 554 10. Rossow, W. B. and Schiffer, R. A.: Advances in understanding clouds from ISCCP. *Bull. Am. Met. Soc.*,  
555 **1999**, 80, 2261–2287.
- 556 11. Ohring, G., Wielicki, B., Spencer, R., Emery, B., and Datla, R. Satellite instrument calibration for  
557 measuring global climate change, *Bull. Amer. Met. Soc.*, **2005**, 86, 1303–1313.
- 558 12. Stengel, M., Stapelberg, S., Sus, O., Schlundt, C., Poulsen, C., Thomas, G., Christensen, M., Carbajal  
559 Henken, C., Preusker, R., Fischer, J., Devasthale, A., Willén, U., Karlsson, K.-G., McGarragh, G.,  
560 Povey, A., Grainger, D., Proud, S., Meirink, J. F., Feofilov, A., Bennartz, R., Bojanowski, J. and  
561 Hollmann, R. Cloud property datasets retrieved from AVHRR, MODIS, AATSR and MERIS in the  
562 framework of the Cloud\_cci project, submitted to Earth System Science Data, **2017**.
- 563 13. Hollmann, R., Merchant, C., Saunders, R., Downy, C., Buchwitz, M., Cazenave, A., Chuvieco, E.,  
564 Defourny, P., de Leeuw, G., Forsberg, R., et al. The ESA climate change initiative: Satellite data  
565 records for essential climate variables, *Bull. Amer. Met. Soc.*, **2013**, 94, 1541–1552.
- 566 14. Stengel, M., Mieruch, S., Jerg, M., Karlsson, K.-G., Scheirer, R., Maddux, B., Meirink, J., Poulsen, C.,  
567 Siddans, R., Walther, A., et al. The clouds climate change initiative: Assessment of state-of-the-art  
568 cloud property retrieval schemes applied to AVHRR heritage measurements, *Rem. Sens. Env.*, **2015**,  
569 162, 363–379.
- 570 15. Devasthale, A., Raspaud, M., Dybbroe, A., Hörnquist, S. and Karlsson, K.-G. PyGAC: an open-source,  
571 community-driven Python interface to preprocess more than 30-yr AVHRR Global Area Coverage  
572 (GAC) data. In preparation.
- 573 16. Woolliams, E., Mittaz, J., Merchant, C. and Dilo, A. Harmonization and Recalibration: A FIDUCEO  
574 perspective. *GSICS Newsletter*, **2016**, Summer Issue, Vol. 10, doi:10.7289/V5GT5K7S.
- 575 17. [A Consistent Long-Term Cloud and Clear-Sky Radiation Property Dataset from the Advanced Very](http://www.ncdc.noaa.gov/cdr/operationalcdrs.html)  
576 [High Resolution Radiometer \(AVHRR\)- Climate Algorithm Theoretical Basis Document, NOAA](http://www.ncdc.noaa.gov/cdr/operationalcdrs.html)  
577 [Climate Data Record Program CDRP-ATBD-0826 Rev. 1 \(2016\). Available at](http://www.ncdc.noaa.gov/cdr/operationalcdrs.html)  
578 <http://www.ncdc.noaa.gov/cdr/operationalcdrs.html>
- 579 16-18.
- 580

